MAJOR PAPER

Differentiating between Glioblastoma and Primary CNS Lymphoma Using Combined Whole-tumor Histogram Analysis of the Normalized Cerebral Blood Volume and the Apparent Diffusion Coefficient

Shixing Bao[1], Yoshiyuki Watanabe[1*], Hiroto Takahashi[1], Hisashi Tanaka[1],
Atsuko Arisawa[1], Chisato Matsuo[1], Rongli Wu[1], Yasunori Fujimoto[2],
and Noriyuki Tomiyama[1]

Purpose: This study aimed to determine whether whole-tumor histogram analysis of normalized cerebral blood volume (nCBV) and apparent diffusion coefficient (ADC) for contrast-enhancing lesions can be used to differentiate between glioblastoma (GBM) and primary central nervous system lymphoma (PCNSL).

Methods: From 20 patients, 9 with PCNSL and 11 with GBM without any hemorrhagic lesions, underwent MRI, including diffusion-weighted imaging and dynamic susceptibility contrast perfusion-weighted imaging before surgery. Histogram analysis of nCBV and ADC from whole-tumor voxels in contrast-enhancing lesions was performed. An unpaired *t*-test was used to compare the mean values for each type of tumor. A multivariate logistic regression model (LRM) was performed to classify GBM and PCNSL using the best parameters of ADC and nCBV.

Results: All nCBV histogram parameters of GBMs were larger than those of PCNSLs, but only average nCBV was statistically significant after Bonferroni correction. Meanwhile, ADC histogram parameters were also larger in GBM compared to those in PCNSL, but these differences were not statistically significant. According to receiver operating characteristic curve analysis, the nCBV average and ADC 25th percentile demonstrated the largest area under the curve with values of 0.869 and 0.838, respectively. The LRM combining these two parameters differentiated between GBM and PCNSL with a higher area under the curve value (Logit $(P) = -21.12 + 10.00 \times$ ADC 25th percentile $(10^{-3}$ mm^2/s) $+ 5.420 \times$ nCBV mean, $P < 0.001$).

Conclusion: Our results suggest that whole-tumor histogram analysis of nCBV and ADC combined can be a valuable objective diagnostic method for differentiating between GBM and PCNSL.

Keywords: *apparent diffusion coefficient, glioblastoma, normalized cerebral blood volume, primary central nervous system lymphoma, whole-tumor histogram analysis*

Introduction

Magnetic resonance imaging features of primary central nervous system lymphoma (PCNSL) and glioblastoma (GBM) are highly variable and sometimes similar,[1,2] complicating differentiation solely by conventional MRI.

[1]Department of Diagnostic and Interventional Radiology, Osaka University Graduate School of Medicine, 2-2 Yamadaoka, Suita, Osaka 565-0871, Japan
[2]Department of Neurosurgery, Osaka University Graduate School of Medicine, Osaka, Japan
*Corresponding author, Phone: +81-6-6879-3434, Fax: +81-6-6879-3439, E-mail: watanabe@radiol.med.osaka-u.ac.jp

Maximum safe resection is regarded as a standard treatment for GBM,[3] while resection in PCNSL is not encouraged because of poor survival benefits and high risk of postoperative deterioration.[4,5] In order to provide distinct, specific surgical plans, and optimal treatments for GBM and PCNSL, preoperative differential diagnosis is quite important.

Many previous studies have aimed to differentiate GBM from PCNSL using conventional MRI[6] and advanced imaging, such as diffusion-weighted imaging (DWI), diffusion tensor imaging (DTI),[7,8] perfusion MRI,[9–12] and texture analysis.[13] The effectiveness of apparent diffusion coefficient (ADC) maps derived from DWI in differentiating PCNSL from GBM has been emphasized by several studies.[14–16] Owing to its higher cellularity, PCNSL has been shown to present lower ADC values than GBM. Dynamic susceptibility

contrast (DSC) perfusion studies have also suggested the differential value of cerebral blood volume (CBV).[17,18] Histogram analyses of normalized CBV (nCBV) and ADC values from the entire tumor volume have already been applied as quantitative techniques in a number of neuroimaging studies.[19–21] Recently, multiparametric imaging has been used to differentiate brain tumors,[22,23] but few studies have combined multiple methods of histogram analysis.

In this study, we aimed to combine DWI–ADC maps and nCBV with whole-tumor histogram analysis. The purpose of this study was to explore the potential use of the ADC–CBV combination model as a tool to discriminate GBM from PCNSL.

Materials and Methods

Patients

Magnetic resonance imaging examinations of 34 consecutive patients (23 men, 11 women; age range 35–79 years; mean age 60.9 ± 11.6 years) with a diagnosis of GBM or PCNSL were evaluated retrospectively. All patients had a previously untreated solitary enhancing brain tumor larger than 2 cm and had undergone routine brain MRI, DSC perfusion-weighted imaging (DSC-PWI), and DWI examination before surgical resection at our hospital between 2009 and 2012. Patients' tumors fulfilled the 2007 World Health Organization (WHO) histopathologic criteria for diagnosis. Fourteen patients with hemorrhagic tumors were excluded from the study because intratumoral hemorrhage may cause considerable signal loss in DSC–PWI images and inaccurate whole-tumor histogram distribution.

The final diagnosis was based on intraoperative observations and histopathologic findings. Of the 20 patients without hemorrhage, WHO grade IV GBM was diagnosed in 11 patients (9 men, 2 women; mean age 60.7 ± 13.8 years; range 35–76 years) and PCNSL was diagnosed in 9 patients (4 men, 5 women; mean age 61.2 ± 12.2 years; range 44–79 years). Institutional review board (IRB) approval was obtained for this research from our hospital. The written informed consent requirement was waived by the IRB, given the retrospective nature of the study.

MRI and image analysis

All MRI examinations were performed within 7 days before surgery. The precontrast sequence consisted of axial T_1-weighted image (T_1WI), T_2-weighted image (T_2WI), DWI, and fluid-attenuated inversion recovery (FLAIR). Once the precontrast imaging was completed, 0.2 mL/kg gadolinium (Gd)-based MR contrast agent (gadoterate meglumine, MAGNESCOPE; Guerbet, Tokyo, Japan) at a rate of 3 mL/s was administered without preload by an MRI-compatible power injector (Spectris; Medrad, Pittsburgh, PA, USA) followed by a 30-mL bolus of saline flush. Postcontrast 3D T_1WIs were obtained immediately after DSC-PWI. All patients were scanned on a 3T scanner (Signa Excite HDxt; GE Healthcare, Milwaukee, USA) with an 8-channel head coil. A DWI using spin echo (SE) echo-planar imaging (EPI) sequence was performed with TR/TE = 6,000/90 ms, FA = 90°, slice thickness = 5 mm, b = 0, 1,000, FOV = 240 mm, matrix = 128 × 128, 20 slices per 1 mm gap. A DSC-PWI using the gradient-echo EPI (GRE-EPI) sequence was performed with TR/TE = 2,000/21 ms, FA = 60°, matrix 96 × 128; FOV, 220 mm; slice thickness = 5 mm, 20 slices per 1 mm gap.

Post-processing

Dynamic susceptibility contrast-perfusion-weighted imaging and conventional MRI data were transferred from the MRI scanner to an independent personal computer for quantitative perfusion and diffusion analysis. Perfusion and diffusion parametric maps were analyzed using the commercially available software nordicICE, (Version 2, NordicNeuroLab AS, Bergen, Norway) to obtain nCBV and ADC maps. For quantitative analysis of the lesion, a relative CBV (rCBV) map with the elimination of recirculation, leakage correction,[24] and vessel-removed using clustering method[25] was calculated. Tracer kinetic models[26,27] were set to make the rCBV maps generated from the area under $1/T_2^*$ converted first-pass curves. The effects of recirculation of contrast agent were reduced by fitting an x variate function to the change in the relaxation rate $(1/T_2^*)$ curve to approximate the curve that would appear without recirculation or leakage. Mathematical correction[24] were made to the dynamic curves to reduce extravascular contrast agent leakage effects. Then, nCBV maps were calculated by dividing the mean rCBV value of the lesion by the mean normal brain tissue rCBV value to minimize variances in an individual patient. Mean normal brain tissue rCBV value was created by normalizing all CBV pixels to the mean CBV value from normal-appearing white and gray matter tissues referenced automatically by the nordicICE. The ADC was calculated from DWI images using nordicICE DWI analysis.

Tumor segmentation of the contrast-enhanced area was acquired according to enhanced tumor mass from the 3D-T_1W-contrast enhanced (CE) image. Overlay image registration was performed for both nCBV and ADC images to match the 3D-T_1W-CE axial images by nordicICE automatically. One neuroradiology resident (S.B) with 3 years of experience independently defined ROI around the entire region of a contrast-enhancing lesion in each section of postcontrast T_1WIs. Circle ROI was drawn around the enhanced lesion and the enhanced lesion was segmented automatically for setting the lesion of interest. Cysts and necrotic parts were not included in the segmentation. The observation results were confirmed by one senior neuroradiologist with 24 years of experience. The setting ROI by enhanced T_1W image was copied to ADC and nCBV maps. If multiple lesions were present, only the largest one was selected. Figures 1 and 2 show this process.

Histogram analysis

The tumor volume of interest was applied to the ADC and nCBV map and each pixel values of tumor segmentation were
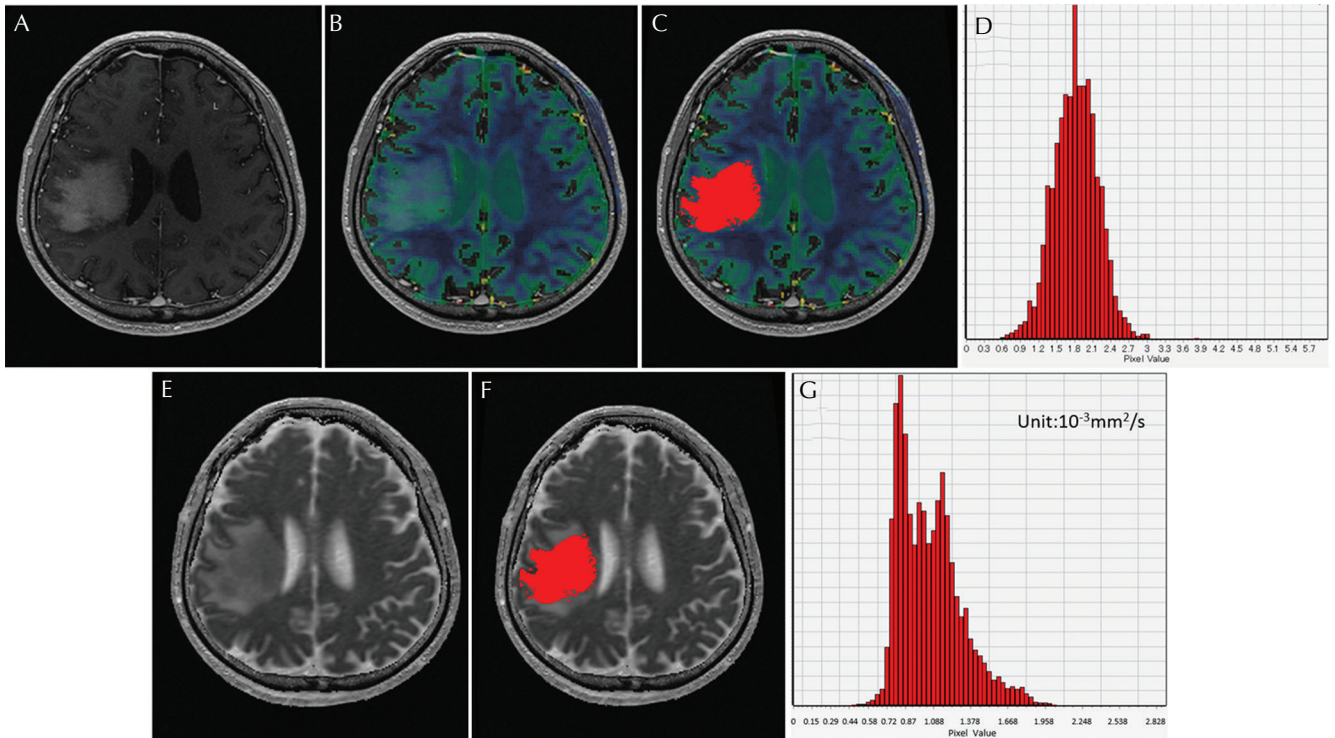
Fig. 1 A 57-year-old male patient with primary central nervous system lymphoma. Normalized cerebral blood volume (nCBV) and apparent diffusion coefficient (ADC) images were overlaid with T_1-weighted contrast-enhanced image (**A**) to form combined image with nCBV (**B**) or ADC (**E**). Segmentation buffers were then loaded to combined image to obtain the volume of interest area (**C**) and (**F**) and yield the histogram result (**D**) and (**G**).
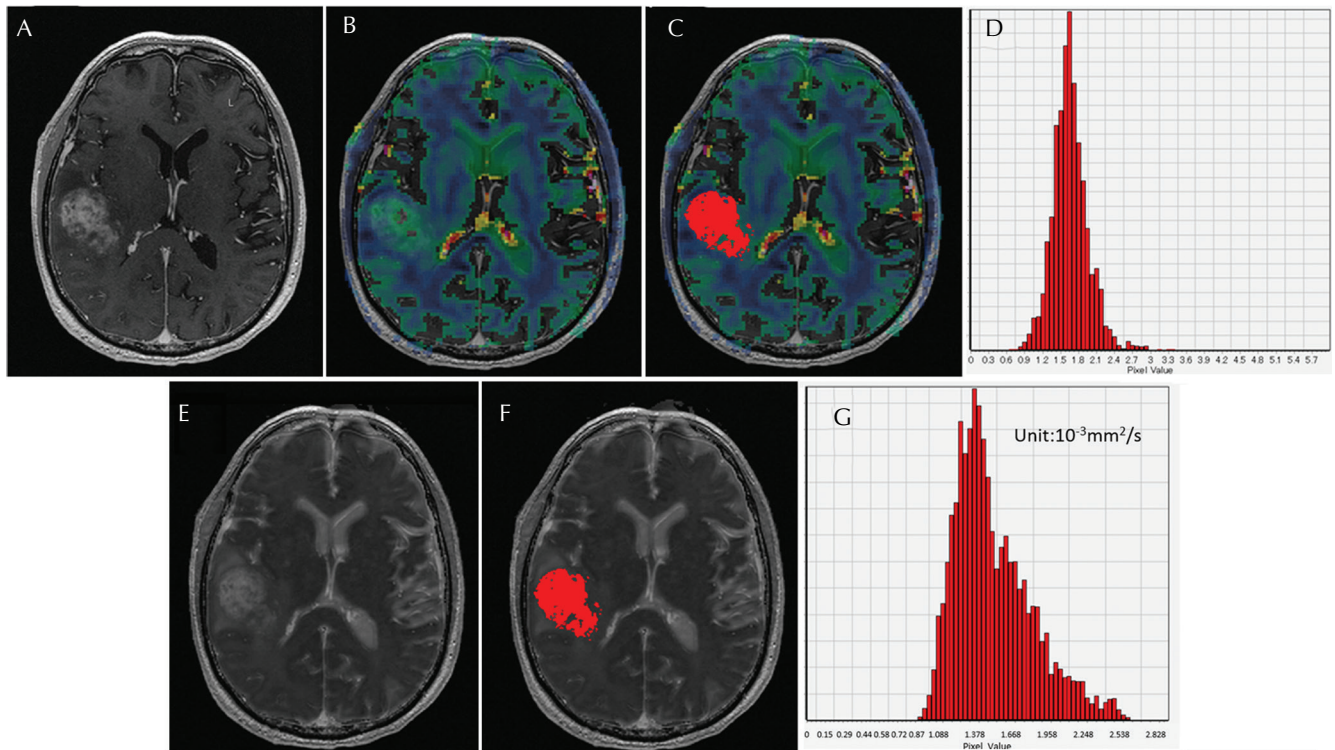

Fig. 2 A 75-year-old male patient with glioblastoma. Normalized cerebral blood volume and apparent diffusion coefficient images were overlaid with T_1-weighted contrast-enhanced image (**A**) to form combined images (**B**) and (**E**). Segmentation buffers were then loaded to combined image to obtain the volume of interest area (**C**) and (**F**) and yield the histogram result (**D**) and (**G**).

measured. Histograms were generated by classification of the ADC and nCBV in whole tumor volume into an optimal number of bins defined by nordicICE software. The distributions of diffusion and perfusion characteristics in the contrast-enhancing lesions of tumors were assessed by the measurement of the average, standard deviation (SD), skewness, kurtosis, minimum, maximum, and 2.5, 25, 50, 75, and 97.5th percentiles. Previous research mention that the maximum rCBV[7,10,28] or the mean CBV[7,18] are valuable for differentiation of GBM and PCNSL and other studies show that minimum ADC[14,29] and mean ADC[8] are valuable for differentiation of GBM and PCNSL, which may suggest that mean to high percentile of CBV and low percentile to mean of ADC values were capable for the distinguishing GBM and lymphoma. Among these parameters, average, SD, skewness, kurtosis, minimum, and 2.5, 25, and 50th percentiles were considered typical for ADC, while average, SD, skewness, kurtosis, maximum, and 50, 75, and 97.5th percentiles were considered typical for nCBV.

Statistical analysis

An unpaired t-test was used to compare the difference in each histogram parameter between GBM and PCNSL. The Receiver operating characteristic (ROC) curve analyses were performed to determine optimum thresholds and the diagnostic accuracy of each histogram parameter for discrimination of the two types of tumors. These analyses permitted the determination of the sensitivity and specificity with each histogram parameter as a function of the threshold value used to discriminate between the two types of tumors. A multivariate linear logistic regression model (LRM) was performed to classify GBM and PCNSL using the best parameter of ADC and nCBV. The purpose of LRM in our study is to predict a possibility of GBM (p), which is depend on ADC and nCBV values of largest AUC.

$$\text{Logit } (p) = \ln (p/1 - p) = a + bX_1 + cX_2 \ (0 < p < 1)$$

X_1 stands for ADC parameter with largest AUC, X_2 stands for nCBV parameter with largest AUC.

All statistical analyses were conducted using IBM SPSS Statistics, version 20.0.0 (IBM Corporation, Armonk, NY, USA). The significance level for the comparison of each histogram parameter was set at 0.05 and the Bonferroni correction was applied to the statistical results to reduce type-I errors generated by multiple comparisons. Since there were eight histogram parameters, P values of <0.00625 (0.05/8) were considered statistically significant.

Results

All nCBV histogram parameters of GBMs were larger than those of PCNSLs (Table 1), but only average nCBV of GBM (2.31 ± 0.60) was significantly larger than PCNSL (1.66 ± 0.38, $P = 0.0056$) after Bonferroni correction. Similarly, ADC histogram values were also larger in GBMs compared

to those in PCNSLs, but these differences were not statistically significant (Table 2). Figures 1: GBM and 2: PCNSL show representative nCBV, ADC, and histograms.

The ROC analysis performed with respect to the GBM and PCNSL groups revealed that the average nCBV and 25th percentile of ADC showed the largest area under the curve (AUC) of 0.869 (sensitivity 72.7%, specificity 88.9%) and 0.838 (sensitivity 72.7%, specificity 88.9%), respectively. Tables 3 and 4 show AUC of all the parameters about nCBV and ADC, respectively, in ROC analysis. Table 5 and Fig. 3 show the ROC-based quantitative comparison of ADC and nCBV parameters.

The LRM combining the 25th percentile of ADC and average nCBV was able to differentiate between GBM and PCNSL with a higher AUC value (AUC = 0.969, sensitivity 88.9%, specificity 90.9%, Logit (p) = −21.12 + 10.00 × ADC 25th percentile (10^{-3} mm²/s) + 5.420 × nCBV mean ($P < 0.001$). Figure 4 shows the scatter plots of the 25th percentile of ADC and average nCBV, as well as threshold line of $P = 0.5$, which can differentiate GBM from PCNSL exist $\ln(p/1 - p) = 0$, and cut-off value of 25th percentile ADC and average nCBV.

Table 1 Mean ± SD of nCBV histogram parameters for GBM and PCNSL

nCBV	GBM	PCNSL	P-value
Average	2.31 ± 0.60	1.66 ± 0.38	0.0056
SD	0.78 ± 0.43	0.46 ± 0.18	0.0627
Skewness	1.30 ± 0.79	0.77 ± 0.92	0.1029
Kurtosis	4.86 ± 7.06	2.18 ± 3.39	0.2706
Maximum	6.94 ± 3.07	4.31 ± 2.97	0.0088
50% tile	2.18 ± 0.52	1.60 ± 0.37	0.007
75% tile	2.71 ± 0.81	1.91 ± 0.48	0.007
97.5% tile	4.23 ± 1.67	2.67 ± 0.78	0.0167

GBM, glioblastoma; nCBV, normalized cerebral blood volume; PCNSL, primary central nervous system lymphoma; SD, standard deviation.

Table 2 Mean ± SD of ADC histogram parameters for GBM and PCNSL

ADC	GBM	PCNSL	P-value
Average	1.48 ± 0.30	1.20 ± 0.27	0.0367
SD	0.34 ± 0.15	0.33 ± 0.13	0.7324
Skewness	1.33 ± 0.59	1.18 ± 0.77	0.5184
Kurtosis	3.75 ± 2.80	3.43 ± 6.15	0.3423
Minimum	0.76 ± 0.19	0.65 ± 0.13	0.1599
2.5% tile	1.00 ± 0.18	0.78 ± 0.15	0.0135
25% tile	1.25 ± 0.23	0.95 ± 0.21	0.0109
50% tile	1.42 ± 0.29	1.12 ± 0.26	0.0367

ADC values (× 10^{-3} mm²/s). ADC, apparent diffusion coefficient; GBM, glioblastoma; nCBV, normalized cerebral blood volume; PCNSL, primary central nervous system lymphoma; SD, standard deviation.

Table 3 Area under the curve (AUC) of all nCBV parameters in ROC analysis

Parameters	AUC	Standard error	Significance (P)	Gradual 95% confidence interval	
				Lower limit	Upper limit
Average	0.869	0.084	0.006	0.704	1.000
SD	0.747	0.116	0.063	0.521	0.974
Skewness	0.717	0.120	0.102	0.482	0.952
Kurtosis	0.646	0.132	0.271	0.387	0.906
Maximum	0.848	0.105	0.009	0.643	1.000
50% tile	0.859	0.087	0.007	0.688	1.000
75% tile	0.859	0.087	0.007	0.689	1.000
97.5% tile	0.818	0.098	0.017	0.626	1.000

Significance shows at $P < 0.05$. nCBV, normalized cerebral blood volume; ROC, receiver operating characteristic; SD, standard deviation.

Table 4 Area under the curve (AUC) of all ADC parameters in ROC analysis

Parameters	AUC	Standard error	Significance (P)	Gradual 95% confidence interval	
				Lower limit	Upper limit
Average	0.778	0.108	0.037	0.566	0.990
SD	0.545	0.136	0.732	0.279	0.812
Skewness	0.586	0.136	0.518	0.320	0.852
Kurtosis	0.626	0.138	0.342	0.356	0.897
Minimum	0.687	0.122	0.160	0.447	0.926
2.5% tile	0.828	0.098	0.014	0.636	1.000
25% tile	0.838	0.094	0.011	0.655	1.000
50% tile	0.778	0.109	0.037	0.564	0.991

Significance shows at $P < 0.05$. ROC, receiver operating characteristic; SD, standard deviation.

Table 5 Receiver operating characteristic analysis of ADC and nCBV values between GBM and PCNSL

Parameter	Sensitivity (%)	Specificity (%)	AUC	Cut-off
ADC 25%	72.7	88.9	0.838	1.02
nCBV average	72.7	88.9	0.869	1.87
ADC + nCBV	88.9	90.9	0.969	

Unit of cut-off value of ADC: $(10^{-3}$ mm^2/s). ADC, apparent diffusion coefficient; AUC, area under the curve; GBM, glioblastoma; nCBV, normalized cerebral blood volume; PCNSL, primary central nervous system lymphoma.

Discussion

Using whole-tumor histogram analysis of ADC and nCBV, we showed that the ADC and nCBV values of GBM were higher than those of PCNSL. Furthermore, the multiparametric image using both ADC and nCBV could improve the diagnostic accuracy of differentiating GBMs from PCNSLs. Few studies have combined ADC and nCBV values to differentiate GBMs from PCNSLs, and
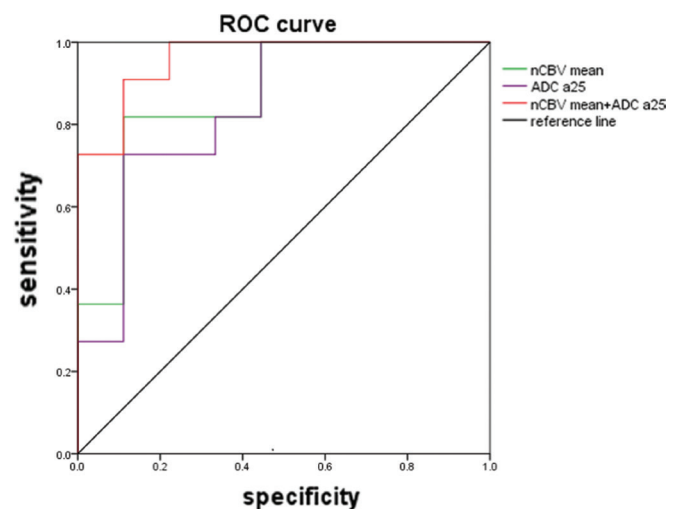

Fig. 3 Receiver operating characteristic curves of the average normalized cerebral blood volume (nCBV), 25th percentile apparent diffusion coefficient (ADC) and combination of average nCBV and 25th percentile ADC. The areas under the curve are 0.869, 0.838, and 0.969, respectively.
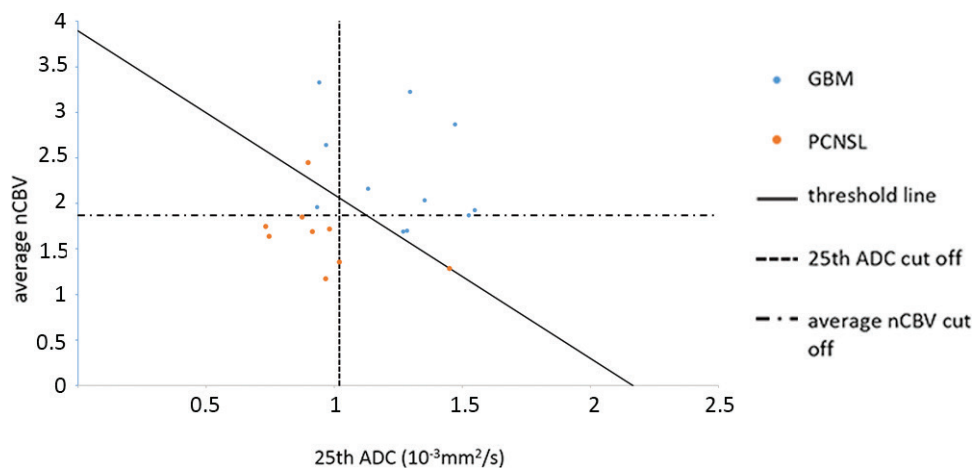
Fig. 4 The scatter plots of the 25th percentile apparent diffusion coefficient (ADC) and average normalized cerebral blood volume (nCBV) of glioblastoma (GBM) and primary central nervous system lymphoma (PCNSL). The threshold line (straight line) turn out to differentiate GBM from PCNSL well when $P = 0.5$. Dotted lines show the cut-off of 25th percentile ADC and average nCBV, respectively.

the present study is the first to do so using histogram parameters.

Several studies have demonstrated that histogram analyses adapted to CBV or ADC values are superior or comparable to the visually guided ROI-based method for distinguishing tumor type,[11,12,20,30] glioma grading,[21,31–33] and recurrence of glioma[34–38] and can provide multiple useful parameters in addition to mean and maximum value. Manual ROI methods to evaluate CBV and ADC were highly operator-dependent, and whole-tumor histogram analysis using semi-automatic tumor definition is quantitative and reproducible.[39–41] In our study, we used eight main histogram parameters derived from nCBV and ADC to differentiate GBMs from PCNSLs. We found that the most significantly distinct parameters between the two types of tumors were the average nCBV and the 25th percentile of ADC according to histogram analysis.

Apparent diffusion coefficient is regarded as a sensitive, specific, and accurate tool to differentiate brain tumor types.[22] Many previous reports differentiated GBM from PCNSL using diffusion parameters.[7,8,12,14,18,39,42] Lin et al.[14] reported that the ADC average had the largest AUC up to 0.826 among all other histogram parameters, regarding this value as a standard to distinguish GBMs from PCNSLs with the average of PCNSLs significantly lower than that of GBMs. Our findings, to a certain extent, agree with this result, except that we found the 25th percentile of ADC with an AUC of 0.838 to be more sensitive.

Average nCBV was the most sensitive parameter in the differential diagnosis of GBMs from PCNSLs and showed the highest AUC in the ROC analysis, with the nCBV of GBM significantly higher than that of PCNSL. This result is consistent with many previous reports, though CBV parameters, such as mean CBV value,[7,18] maximum CBV value,[20,28,43] and 80th percentile of CBV[11] have been shown to be variable. Our results showed that the maximum CBV of PCNSLs tended to be significantly lower than that of GBMs, with a large AUC of 0.848. This result is consistent with findings of previous MR perfusion studies for PCNSL.[10,28]

Ma et al.[20] described whole-tumor histogram analysis of nCBV in GBM, PCNSL, and solitary brain metastasis. They used three histogram parameters: peak height position, maximum value, and histogram width. With respect to differentiation between GBM and PCNSL, the histogram width and maximum value showed sensitivity and specificity of 100%. The difference between this study and others may be related to different patient selection methods.

Many previous studies aiming to differentiate GBM from PCNSL used PWI and DWI because advanced brain tumor imaging includes both of these.[12,18,29,30,44] While most studies have only compared DWI and PWI results, some have combined these results to distinguish GBM from PCNSL.[7,11,18] Recently, multiparametric imaging has been used to differentiate brain tumor types, and with advances in analysis software, multiparametric imaging is a promising tool for distinguishing tumor characteristics.[18,23,35,45–49] In our results, the 25th percentile of ADC and the mean of nCBV values overlapped in many cases (Fig. 4), but combining these two parameters with DWI and CBV more accurately differentiated GBM and PCNSL and raised the AUC value to 0.932.

High cellular situation can contribute to low ADC value, as well as high blood supply stand for high nCBV value. According to our result, PCNSL showed higher cellular situation and lower blood volume of the tumor capillaries and venules per tissue volume compared to GBM. In our study, 25% ADC and average nCBV had the largest AUC compared to other ADC and nCBV parameters. For histogram analysis, the maximum and minimum values represent one voxel value, which most likely includes some artifacts. The percentile values excluded these outliers. For ADC analysis, 25th percentile ADC and 2.5th percentile ADC showed high AUC values, which suggest that high cellularity part of tumors could discriminate between GBM and PCNSL. For nCBV analysis, average, median, and 75th percentile nCBV showed high AUC values, which demonstrate that the whole tumor blood volume is higher in GBM compared to PCNSL.

Our study has several potential limitations. First, to eliminate the influence of hemorrhage, which is quite common in GBM cases, nearly, half of the GBM cases were excluded

from analysis. As such, the number of patients was small, and including more patients would have strengthened the statistical power. Second, we segmented the enhanced tumor using threshold methods and nCBV value are estimated by the large-vessel-removed using the cluster analysis, but the including the vessel components in the tumors were fully not excluded. Furthermore, while some studies have evaluated the perienhancing tumor region, we evaluated only enhanced areas. The optimal definition of the perienhancing tumor region is complicated because gliomas are infiltrating tumors with indistinct borders beyond the radiologic margins.[50,51] At last, larger tumors will have a greater impact on total tumor perfusion and diffusion metrics compared with smaller tumors in whole-tumor analysis. Further studies with larger populations and more accurate tumor size classification are necessary to validate the value of histogram parameters in tumor type differentiation.

Conclusion

Our results suggest that whole-tumor histogram analysis combining nCBV and ADC can be a valuable objective diagnostic method for differentiating between GBM and PCNSL.

Conflicts of Interest

The authors declare that they have no conflicts of interest.

References

1. Koeller KK, Smirniotopoulos JG, Jones RV. Primary central nervous system lymphoma: radiologic–pathologic correlation. Radiographics 1997; 17:1497–1526.
2. Rees JH, Smirniotopoulos JG, Jones RV, Wong K. Glioblastoma multiforme: radiologic–pathologic correlation. Radiographics 1996; 16:1413–1438.
3. Marko NF, Weil RJ, Schroeder JL, Lang FF, Suki D, Sawaya RE. Extent of resection of glioblastoma revisited: personalized survival modeling facilitates more accurate survival prediction and supports a maximum-safe-resection approach to surgery. J Clin Oncol 2014; 32:774–782.
4. Bataille B, Delwail V, Menet E, et al. Primary intracerebral malignant lymphoma: report of 248 cases. J Neurosurg 2000; 92:261–266.
5. DeAngelis LM. Primary CNS lymphoma: treatment with combined chemotherapy and radiotherapy. J Neurooncol 1999; 43:249–257.
6. Malikova H, Koubska E, Weichet J, et al. Can morphological MRI differentiate between primary central nervous system lymphoma and glioblastoma? Cancer Imaging 2016; 16:40.
7. Wang S, Kim S, Chawla S, et al. Differentiation between glioblastomas, solitary brain metastases, and primary cerebral lymphomas using diffusion tensor and dynamic susceptibility contrast-enhanced MR imaging. AJNR Am J Neuroradiol 2011; 32:507–514.
8. Toh CH, Castillo M, Wong AM, et al. Primary cerebral lymphoma and glioblastoma multiforme: differences in diffusion characteristics evaluated with diffusion tensor imaging. AJNR Am J Neuroradiol 2008; 29:471–475.
9. Toh CH, Wei KC, Chang CN, Ng SH, Wong HF. Differentiation of primary central nervous system lymphomas and glioblastomas: comparisons of diagnostic performance of dynamic susceptibility contrast-enhanced perfusion MR imaging without and with contrast-leakage correction. AJNR Am J Neuroradiol 2013; 34:1145–1149.
10. Liao W, Liu Y, Wang X, et al. Differentiation of primary central nervous system lymphoma and high-grade glioma with dynamic susceptibility contrast-enhanced perfusion magnetic resonance imaging. Acta Radiol 2009; 50: 217–225.
11. Murayama K, Nishiyama Y, Hirose Y, et al. Differentiating between central nervous system lymphoma and high-grade glioma using dynamic susceptibility contrast and dynamic contrast-enhanced MR imaging with histogram analysis. Magn Reson Med Sci 2018; 17:42–49.
12. Choi YS, Lee HJ, Ahn SS, et al. Primary central nervous system lymphoma and atypical glioblastoma: differentiation using the initial area under the curve derived from dynamic contrast-enhanced MR and the apparent diffusion coefficient. Eur Radiol 2017; 27: 1344–1351.
13. Kunimatsu A, Kunimatsu N, Kamiya K, Watadani T, Mori H, Abe O. Comparison between glioblastoma and primary central nervous system lymphoma using MR image-based texture analysis. Magn Reson Med Sci 2018; 17:50–57.
14. Lin X, Lee M, Buck O, et al. Diagnostic accuracy of T_1-weighted dynamic contrast-enhanced-MRI and DWI-ADC for differentiation of glioblastoma and primary CNS lymphoma. AJNR Am J Neuroradiol 2017; 38: 485–491.
15. Guo AC, Cummings TJ, Dash RC, Provenzale JM. Lymphomas and high-grade astrocytomas: comparison of water diffusibility and histologic characteristics. Radiology 2002; 224:177–183.
16. Doskaliyev A, Yamasaki F, Ohtaki M, et al. Lymphomas and glioblastomas: differences in the apparent diffusion coefficient evaluated with high b-value diffusion-weighted magnetic resonance imaging at 3T. Eur J Radiol 2012; 81:339–344.
17. Xing Z, You RX, Li J, Liu Y, Cao DR. Differentiation of primary central nervous system lymphomas from high-grade gliomas by rCBV and percentage of signal intensity recovery derived from dynamic susceptibility-weighted contrast-enhanced perfusion MR imaging. Clin Neuroradiol 2014; 24:329–336.
18. Kickingereder P, Wiestler B, Sahm F, et al. Primary central nervous system lymphoma and atypical glioblastoma: multiparametric differentiation by using diffusion-, perfusion-, and susceptibility-weighted MR imaging. Radiology 2014; 272:843–850.
19. Arisawa A, Watanabe Y, Tanaka H, et al. Vessel-masked perfusion magnetic resonance imaging with histogram analysis improves diagnostic accuracy for the grading of glioma. J Comput Assist Tomogr 2017; 41:910–915.
20. Ma JH, Kim HS, Rim NJ, Kim SH, Cho KG. Differentiation among glioblastoma multiforme, solitary metastatic tumor, and lymphoma using whole-tumor histogram analysis of

the normalized cerebral blood volume in enhancing and perienhancing lesions. AJNR Am J Neuroradiol 2010; 31:1699–1706.

21. Emblem KE, Nedregaard B, Nome T, et al. Glioma grading by using histogram analysis of blood volume heterogeneity from MR-derived cerebral blood volume maps. Radiology 2008; 247:808–817.

22. Kimura M, da Cruz LCH. Multiparametric MR imaging in the assessment of brain tumors. Magn Reson Imaging Clin N Am 2016; 24:87–122.

23. Bauer AH, Erly W, Moser FG, Maya M, Nael K. Differentiation of solitary brain metastasis from glioblastoma multiforme: a predictive multiparametric approach using combined MR diffusion and perfusion. Neuroradiology 2015; 57:697–703.

24. Boxerman JL, Schmainda KM, Weisskoff RM. Relative cerebral blood volume maps corrected for contrast agent extravasation significantly correlate with glioma tumor grade, whereas uncorrected maps do not. AJNR Am J Neuroradiol 2006; 27:859–867.

25. Emblem KE, Due-Tonnessen P, Hald JK, Bjornerud A. Automatic vessel removal in gliomas from dynamic susceptibility contrast imaging. Magn Reson Med 2009; 61:1210–1217.

26. Ostergaard L, Weisskoff RM, Chesler DA, Gyldensted C, Rosen BR. High resolution measurement of cerebral blood flow using intravascular tracer bolus passages. Part I: Mathematical approach and statistical analysis. Magn Reson Med 1996; 36:715–725.

27. Rosen BR, Belliveau JW, Vevea JM, Brady TJ. Perfusion imaging with NMR contrast agents. Magn Reson Med 1990; 14:249–265.

28. Hartmann M, Heiland S, Harting I, et al. Distinguishing of primary cerebral lymphoma from high-grade glioma with perfusion-weighted magnetic resonance imaging. Neurosci Lett 2003; 338:119–122.

29. Yamashita K, Yoshiura T, Hiwatashi A, et al. Differentiating primary CNS lymphoma from glioblastoma multiforme: assessment using arterial spin labeling, diffusion-weighted imaging, and ^{18}F-fluorodeoxyglucose positron emission tomography. Neuroradiology 2013; 55:135–143.

30. Nakajima S, Okada T, Yamamoto A, et al. Primary central nervous system lymphoma and glioblastoma: differentiation using dynamic susceptibility-contrast perfusion-weighted imaging, diffusion-weighted imaging, and ^{18}F-fluorodeoxyglucose positron emission tomography. Clin Imaging 2015; 39:390–395.

31. Arevalo-Perez J, Peck KK, Young RJ, Holodny AI, Karimi S, Lyo JK. Dynamic contrast-enhanced perfusion MRI and diffusion-weighted imaging in grading of gliomas. J Neuroimaging 2015; 25:792–798.

32. Ryu YJ, Choi SH, Park SJ, Yun TJ, Kim JH, Sohn CH. Glioma: application of whole-tumor texture analysis of diffusion-weighted imaging for the evaluation of tumor heterogeneity. PLoS ONE 2014; 9:e108335.

33. Kang Y, Choi SH, Kim YJ, et al. Gliomas: histogram analysis of apparent diffusion coefficient maps with standard- or high-b-value diffusion-weighted MR imaging—correlation with tumor grade. Radiology 2011; 261:882–890.

34. Rahman R, Hamdan A, Zweifler R, et al. Histogram analysis of apparent diffusion coefficient within enhancing and nonenhancing tumor volumes in recurrent glioblastoma patients treated with bevacizumab. J Neurooncol 2014; 119:149–158.

35. Cha J, Kim ST, Kim HJ, et al. Differentiation of tumor progression from pseudoprogression in patients with posttreatment glioblastoma using multiparametric histogram analysis. AJNR Am J Neuroradiol 2014; 35:1309–1317.

36. Song YS, Choi SH, Park CK, et al. True progression versus pseudoprogression in the treatment of glioblastomas: a comparison study of normalized cerebral blood volume and apparent diffusion coefficient by histogram analysis. Korean J Radiol 2013;14:662–672.

37. Pope WB, Lai A, Mehta R, et al. Apparent diffusion coefficient histogram analysis stratifies progression-free survival in newly diagnosed bevacizumab-treated glioblastoma. AJNR Am J Neuroradiol 2011; 32: 882–889.

38. Pope WB, Kim HJ, Huo J, et al. Recurrent glioblastoma multiforme: ADC histogram analysis predicts response to bevacizumab treatment. Radiology 2009; 252: 182–189.

39. Ahn SJ, Shin HJ, Chang JH, Lee SK. Differentiation between primary cerebral lymphoma and glioblastoma using the apparent diffusion coefficient: comparison of three different ROI methods. PLoS ONE 2014; 9:e112948.

40. Young R, Babb J, Law M, Pollack E, Johnson G. Comparison of region-of-interest analysis with three different histogram analysis methods in the determination of perfusion metrics in patients with brain gliomas. J Magn Reson Imaging 2007; 26:1053–1063.

41. Law M, Young R, Babb J, Pollack E, Johnson G. Histogram analysis versus region of interest analysis of dynamic susceptibility contrast perfusion MR imaging data in the grading of cerebral gliomas. AJNR Am J Neuroradiol 2007; 28:761–766.

42. Shim WH, Kim HS, Choi CG, Kim SJ. Comparison of apparent diffusion coefficient and intravoxel incoherent motion for differentiating among glioblastoma, metastasis, and lymphoma focusing on diffusion-related parameter. PLoS ONE 2015; 10:e0134761.

43. Rollin N, Guyotat J, Streichenberger N, Honnorat J, Tran Minh VA, Cotton F. Clinical relevance of diffusion and perfusion magnetic resonance imaging in assessing intra-axial brain tumors. Neuroradiology 2006; 48: 150–159.

44. Calli C, Kitis O, Yunten N, Yurtseven T, Islekel S, Akalin T. Perfusion and diffusion MR imaging in enhancing malignant cerebral tumors. Eur J Radiol 2006; 58:394–403.

45. Boonzaier NR, Larkin TJ, Matys T, van der Hoorn A, Yan JL, Price SJ. Multiparametric MR imaging of diffusion and perfusion in contrast-enhancing and nonenhancing components in patients with glioblastoma. Radiology 2017; 284:180–190.

46. Yu Y, Lee DH, Peng SL, et al. Assessment of glioma response to radiotherapy using multiple MRI biomarkers

with manual and semiautomated segmentation algorithms. J Neuroimaging 2016; 26:626–634.

47. Kickingereder P, Bonekamp D, Nowosielski M, et al. Radiogenomics of glioblastoma: machine learning-based classification of molecular characteristics by using multiparametric and multiregional MR imaging features. Radiology 2016; 281:907–918.

48. Akbari H, Macyszyn L, Da X, et al. Imaging surrogates of infiltration obtained via multiparametric imaging pattern analysis predict subsequent location of recurrence of glioblastoma. Neurosurgery 2016; 78:572–580.

49. Park JE, Kim HS, Goh MJ, Kim SJ, Kim JH. Pseudoprogression in patients with glioblastoma: assessment by using volume-weighted voxel-based multiparametric clustering of MR imaging data in an independent test set. Radiology 2015; 275:792–802.

50. Price SJ, Jena R, Burnet NG, et al. Improved delineation of glioma margins and regions of infiltration with the use of diffusion tensor imaging: an image-guided biopsy study. AJNR Am J Neuroradiol 2006; 27:1969–1974.

51. Grier JT, Batchelor T. Low-grade gliomas in adults. Oncologist 2006; 11:681–693.